JNeurosci
THE JOURNAL OF NEUROSCIENCE

Research Articles: Cellular/Molecular

$P2Y_6$ receptor-dependent microglial phagocytosis of synapses during development regulates synapse density and memory

https://doi.org/10.1523/JNEUROSCI.1089-23.2023

Cite as: J. Neurosci 2023; 10.1523/JNEUROSCI.1089-23.2023

Received: 15 May 2023
Revised: 27 July 2023
Accepted: 31 August 2023

$P2Y_6$ receptor-dependent microglial phagocytosis of synapses during development regulates synapse density and memory

Running title: $P2Y_6$ receptor and brain development

Jacob M. Dundee[1], Mar Puigdellívol[1,2], Richard Butler[3], and Guy C. Brown*[1]

[1]Department of Biochemistry, University of Cambridge, Cambridge, United Kingdom
[2]Institute of Neurosciences, University of Barcelona, Barcelona, Spain
[3]The Wellcome Trust Cancer Research UK Gurdon Institute, University of Cambridge, Cambridge, United Kingdom

* Corresponding author: gcb3@cam.ac.uk

Number of pages: 28
Number of figures: 12 (9 in main, 3 extended)

Abstract: 181 words
Introduction: 547 words
Discussion: 1,370 words

Conflict of interest statement
The authors declare no competing interests.

Acknowledgments
We thank Bernard Robaye for the $P2Y_6R$ knockout mice, and Stefan Milde for carrying out the behavioral tests on 9-12-month-old mice. The authors gratefully acknowledge the Cambridge Advanced Imaging Centre for their support & assistance in this work. This work was supported by: the Medical Research Council UK [MR/L010593]; the Biotechnology and Biological Sciences Research Council [BB/T508160/1]; and Eli Lilly [ARUK-DC2017-4 and RG99704].

Abstract

During brain development, excess synapses are pruned (i.e. removed), in part by microglial phagocytosis, and dysregulated synaptic pruning can lead to behavioral deficits. The $P2Y_6$ receptor ($P2Y_6R$) is known to regulate microglial phagocytosis of neurons, and to regulate microglial phagocytosis of synapses in cell culture and *in vivo* during aging. However, currently it is unknown whether $P2Y_6R$ regulates synaptic pruning during development. Here, we show that $P2Y_6R$ knockout mice of both sexes had strongly reduced microglial internalization of synaptic material, measured as Vglut1 within CD68-staining lysosomes of microglia at postnatal day 30 (P30), suggesting reduced microglial phagocytosis of synapses. Consistent with this, we found an increased density of synapses in the somatosensory cortex and the CA3 region and dentate gyrus of the hippocampus at P30. We also show that adult $P2Y_6R$ knockout mice have impaired short- and long-term spatial memory and impaired short- and long-term recognition memory compared to wild-type mice, as measured by novel location recognition, novel object recognition, and Y-maze memory tests. Overall, this indicates $P2Y_6R$ regulates microglial phagocytosis of synapses during development, and this contributes to memory capacity.

Significance statement

The $P2Y_6$ receptor ($P2Y_6R$) is activated by UDP released by neurons, inducing microglial phagocytosis of such neurons or synapses. We tested whether $P2Y_6R$ regulates developmental synaptic pruning in mice and found that $P2Y_6R$ knockout mice have reduced synaptic material within microglial lysosomes, and increased synaptic density in the brains of postnatal day 30 mice, consistent with reduced synaptic pruning during development. We also found that adult $P2Y_6R$ knockout mice had reduced memory, consistent with persistent deficits in brain function, resulting from impaired synaptic pruning. Overall, the results suggest that $P2Y_6R$ mediates microglial phagocytosis of synapses during development, and the absence of this results in memory deficits in the adult.

Introduction

During development, synapse formation in the human brain is thought to peak at 1 million synapses per second (Tang et al., 2001). Excess synapses are generated compared to what remains in adulthood, and some of these synapses are then pruned to shape neuronal networks in an activity-dependent manner (Hong, Dissing-Olesen and Stevens, 2016; Faust, Gunner and Schafer, 2021). This synaptic pruning is by multiple mechanisms but is partly mediated by microglial phagocytosis of the synapses (Stevens et al 2007; Tremblay, Lowery, and Majewska, 2010; Paolicelli et al., 2011; Schafer et al., 2012; Mordelt and de Witte, 2023).

Microglia are macrophages, resident central nervous system, that play a variety of roles in maintaining a healthy brain. One such role involves the phagocytosis (i.e., engulfment and degradation) of synapses, neurons, debris, bacteria, and aggregated proteins (Sierra et al., 2013; Wolf, Boddeke and Kettenmann, 2017; Tay et al., 2018; Gabandé-Rodríguez, Keane and Capasso, 2020). Microglial phagocytosis of synapses is involved in learning and memory in adults (Miyanishi et al., 2021), but excessive microglial phagocytosis of the synapses may contribute to memory loss with aging and neurodegeneration (Hong et al., 2016; Dundee et al., 2023). Signals regulating microglial phagocytosis of synapses include fractalkine and the fractalkine receptor, complement components C1q, C3 and C4 and complement receptor 3, adenosine 2A, TREM2, GPR56, phosphatidylserine, CD47, TGFb, and the $P2Y_6$ receptor ($P2Y_6R$) (Faust, Gunner and Schafer, 2021; Dundee et al., 2023).

$P2Y_6R$ is a G-protein-coupled receptor for extracellular uridine diphosphate (UDP), expressed from the *P2ry6* gene by myeloid and other cells in the body, but in the brain, is almost exclusively expressed by microglia (Koizumi et al., 2007). Koizumi et al. (2007) found that kainite-stressed neurons released uridine triphosphate, which was hydrolyzed into UDP and induced microglia to phagocytose neurons via activating $P2Y_6R$ on microglia. We subsequently showed that extracellular UDP could induce microglia to phagocytose live neurons, and that inhibition of $P2Y_6R$ prevented neuronal loss induced by LPS in glial-neuronal cultures and in mouse brains *in vivo* (Neher et al., 2014; Milde et al., 2021). $P2Y_6R$ knockout also prevented microglial phagocytosis of neurons and loss of neurons and memory induced beta amyloid and TAU *in vivo* (Puigdellívol et al., 2021).

Recently, we reported that $P2Y_6R$ regulated microglial phagocytosis of synapses (Dundee et al., 2023). In culture, we showed that $P2Y_6R$ inhibition or knockout strongly reduced microglial phagocytosis of isolated synapses (synaptosomes), and that glial-neuronal cultures from $P2Y_6R$ knockout mice had reduced inflammatory loss of synapses (Dundee et al., 2023). *In vivo*, we found that $P2Y_6R$ knockout prevented an aging-associated increase in microglial phagocytosis of synapses, and reduced loss of synapses and memory with age (Dundee et al., 2023).

Here, we investigated whether $P2Y_6R$ regulated microglial phagocytosis of synapses during development, and whether this affected synaptic density and memory. We found that microglia from $P2Y_6R$ knockout mice had reduced internalization of synaptic material at postnatal day 30 compared to wild-type mice, coupled with an increase in synaptic density in three different regions of $P2Y_6R$ knockout mouse brains. $P2Y_6R$ knockout mice also performed worse than wild-type mice in both long- and short-term memory tests. These findings are significant as they support the hypothesis that microglial phagocytosis of synapses during development contributes to a healthy brain and this is, in part, through activation of the $P2Y_6R$.

Materials and Methods

Animals

All animal work was carried out in accordance with the Animals (Scientific Procedures) Act 1986 Amendment Regulations 2012 following ethical review by the University of Cambridge Animal Welfare and Ethical Review Body (AWERB). $P2Y_6R$ knockout mice were kindly provided by Bernard Robaye (ULB Brussels) and maintained on a C57BL/6 background (Charles River Laboratories). $P2Y_6R$ knockout mice and wild-type littermates were used to establish homozygous $P2Y_6R$ wild-type and knockout sub-lines. Postnatal day 30 (P30) mice included 4 male and 4 female wild-type mice and 4 male and 4 female $P2Y_6R$ knockout mice. 4-month-old mice included 6 male and 5 female wild-type mice and 8 male and 3 female $P2Y_6R$ knockout mice. 9-12-month-old mice included 9 female wild-type mice and 7 female $P2Y_6R$ knockout mice. Mice utilized in short-term memory tests received intracerebroventricular injections of 4 µL PBS 3 or 14 days prior to testing.

Fixation and tissue sectioning

P30 mice were sacrificed following cervical dislocation and decapitation. Brains were removed and fixed for 48 hours in 4% paraformaldehyde and cryoprotected by immersion in an increased 10%–30% sucrose solution until sectioning. Serial coronal sections (25 µm) through the whole brain were collected using a sliding microtome and placed in PBS with 0.025% sodium azide as free-floating sections.

Immunohistochemistry of free-floating brain slices

All steps were carried out at room temperature, with shaking, and rinsing thrice with PBS after each incubation unless stated otherwise. Five to six free-floating 25 µm sections were taken every 12th brain section of 8 $P2Y_6R$ wild-type and knockout mice at P30 for immunohistochemistry. Sections were rinsed three times in PBS and incubated with 50 mM ammonium chloride in PBS for 30 min to quench free aldehyde groups from fixation. Sections were then incubated in 0.1% Sudan Black B in 70% ethanol for 20 min to reduce autofluorescence, permeabilized using 1% Triton X-100 in PBS for 30 min to facilitate antibody penetration, and blocked for 1 h with blocking solution (2% bovine serum albumin, 3% goat serum, and 0.03% Triton X-100 in PBS). Subsequently, sections were incubated with mouse anti-Vglut1 (1:200, Thermo Fisher, MA5-31373), rabbit anti-Homer1 (1:500, Synaptic Systems, 160003), rabbit anti-Iba1 (1:200, Wako, 019-19741), and rat CD68 (1:200, Thermo Fisher, 14-0681-82) antibodies in blocking solution for 2 h at 37°C (Xiao et al., 2017). Sections were then rinsed three times with PBS and then incubated with Alexa-Fluor 568 goat anti-mouse (1:200, Thermo Fisher, A5054), Alexa-Fluor goat 488 anti-rabbit (1:200, Thermo Fisher, A11008), and Alexa-Fluor 647 goat anti-rat (1:200, Thermo Fisher, A21247) antibodies for 2 h at 37°C. Sections were then rinsed three times with PBS and mounted on poly-l-lysine-treated glass slides and dried at 37°C. Sections were then mounted using Vectashield mounting medium with DAPI (Vector Laboratories, H1500) and imaged using confocal microscopy.

Synaptic internalization analysis of free-floating brain sections

Imaging was carried out on a Nikon C2si confocal microscope with a 63×, 1.35 NA oil immersion objective using 488, 561, and 640 nm laser lines. Microglia were imaged and analyzed following Schafer et al. (2014). Briefly, Z-stacks (0.5 µm step intervals) were collected being 2 µm from the surface of the section at each region of interest. Fourteen to fifteen microglia were analyzed across three sections 300 µm apart per mouse. Background subtraction (six pixels/0.2 µm rolling ball) and intensity normalization (2%) across the sections was carried out using Fiji (Schindelin et al., 2012). Microglial structures were analyzed using 3D Morph analysis (York et al., 2018). Microglial (Iba1), lysosomal (CD68), and synaptic (Vglut1) surface rendering was carried out using Imaris 9.1.2. The results for the surface-rendered objects were represented as volume (μm^3).

Microglial density of free-floating brain sections

Imaging was carried out on an EVOS M5000 fluorescent microscope with a 20× objective. Nine images in the somatosensory cortex were taken across three sections 300 µm apart per mouse. Total microglia (Iba1- and DAPI-positive) per field were counted using Fiji (Schindelin et al., 2012).

Synaptic density analysis of free-floating brain sections

Imaging was carried out on a Nikon C2si confocal microscope with a 63×, 1.35 NA oil immersion objective using 405, 488, and 561 nm laser lines. A 2-µm *Z*-stack (0.125 µm step intervals) was collected being 2–5 µm from the surface of the section at each region of interest. Nine images were taken across three sections 300 µm apart per mouse. Background subtraction (six pixels/0.2 µm rolling ball) and intensity normalization (2%) across the sections were carried out using Fiji (Schindelin et al., 2012). We developed a custom script for Fiji to map Vglut1 and Homer1 puncta positions in 3D and analyze their distributions. In order to detect puncta 0.2 µm in diameter (Moreno Manrique et al., 2021), the script applies a Laplacian of Gaussian filter with the standard deviation set from this estimated diameter and detects local maxima as puncta candidates. Candidate points are then clustered into final puncta by merging points within one punctum width of each other, excluding points on image edges and below the global Otsu intensity threshold (Otsu et al., 1979). The number of puncta "colocalized" between the two channels is counted as the number of C2 (Homer1) coordinates having at least one C3 (Vglut1) coordinate within one punctum width. Local density is calculated for each punctum using a Gaussian kernel density estimate (Davis, Lii and Politis, 1956), and overall density in each channel is calculated as puncta per μm^3. The puncta densities were normalized to the mean of wild-type mice.

Long-term novel object location test and novel object recognition test

To test long-term location and recognition memory, object location recognition testing (OLRT) and novel object recognition testing (NORT) was performed in a 30 × 44 cm arena with opaque sides, with a 24 h retention time (Murai et al., 2007; Puigdellívol et al., 2021). Briefly, 4-month-old mice were first habituated to the arena in the absence of objects on two consecutive days (15 min/day), when spontaneous locomotor activity (total distance traveled) and anxiety/motivation (distance traveled in periphery versus center of the open field) were measured. On the third day, visual clues were included on the walls of the open field and two similar objects were presented for 10 min (A and A' objects). Twenty-four hours later, the same animals were retested for 5 min retention test in the arena with a familiar (A) and a new (B) object location. The object location preference was measured as the time exploring each object × 100/time exploring both objects. On the fifth day, visual clues were removed and two new identical objects were presented to the animals for 10 min (C and C'). Twenty-four hours later, the same animals were retested for 5 min retention test in the arena with a familiar (C) and a new (D) object. The object preference was measured as the time exploring each object × 100/time exploring both objects. Animals were tracked and recorded with SMART Junior software (Panlab). Objects and arena were cleaned thoroughly with 70% ethanol and dried after each trial to eliminate odor cues. Experimenter was blinded to the genotype of the individual animals. NORT data was reanalyzed from Dundee et al. (2023).

Short-term novel object recognition memory test

To test short-term recognition memory, novel object recognition testing (NORT) was performed in a 30 × 44 cm arena with opaque sides, with a 2 min retention time (Puigdellívol et al., 2021). Briefly, 9-12-month-old mice were first habituated to the arena in the absence of objects for two 10 min sessions 2 h apart. The next day, two identical objects were presented for 10 min (A and A' objects). 2 minutes later, the same animals were retested for 5 min in the arena with a familiar (A) and a novel (B) object. The order of testing of mice from different experimental groups was randomized on day 1 and maintained in the same order on day 2. Object interaction times and ratios were extracted from digital recordings of the trials using modified "Autotyping" software. Experimenter was blinded to the genotype of the individual animals. This data was reanalyzed from Puigdellívol et al. (2021).

Y-maze memory test

To test short-term spatial memory, spontaneous alternation performance in a Y-maze was tested as described previously (Prieur and Jadavji, 2019). Briefly, 9-12-month-old mice were placed in the center of the symmetrical Y-maze and were allowed to explore freely through the maze during an 8 min session. The sequence, total number of arms entered, and total distance travelled was recorded. Spontaneous alternations (%) are as follows: number of arm entries that were not identical to the previous arm entry/total number of arm entries × 100. Arm entries and distance travelled were extracted from digital recordings of the trials using modified “Autotyping” software. Experimenter was blinded to the genotype of the individual animals.

Statistical analysis

Bars represent mean ± SEM, and each data point represents one animal (Fig. 1d-f, 2b,d,e-g, 3b, 4d, 5d, 6d, 7d, 8b,c,d,e,f, 9b-d,f,g, and Extended Fig. 4-1a-l, 4-2). Statistical differences were calculated using unpaired *t* tests and one-sample *t* tests. Statistical correlation was carried out using paired Pearson correlation coefficients. All experiments were analyzed using GraphPad Prism 9 (GraphPad software). Graphical data were shown as individual data points, including mean values with error bars indicating SEM. *p*-values of $^{*}p < 0.05$, $^{**}p < 0.01$ indicated significant differences between groups. For each experiment and graph, statistical details including the statistical test used, the exact value of *n*, what *n* represents (number of animals per genotype) as well as dispersion and precision measures (mean, SEM, etc.) can be found in each figure legend.

Results

$P2Y_6R$ knockout results in reduced synaptic internalization during development

During development, synaptic levels are regulated in part by the phagocytosis of synapses by microglia (Schafer et al., 2012). We have previously shown that $P2Y_6R$ knockout microglia have reduced synaptic internalization during aging (Dundee et al., 2023). To test whether $P2Y_6R$ is involved in the microglial phagocytosis of synapses during development, we analyzed the internalization of synaptic material within microglial lysosomes in the somatosensory cortex of P30 wild-type and knockout mice by confocal microscopy (Fig. 1a). Coronal brain slices were immunostained using antibodies to Iba1 (microglial marker), CD68 (lysosomal marker), and Vglut1 (pre-synaptic marker), and internalized Vglut1 volume within lysosomal microglia was analyzed by generating Z-projection surface renderings using Imaris software (Fig. 1b,c). We chose a pre-synaptic marker (Vglut1), rather than a post-synaptic marker, as there is clearer evidence for microglial phagocytosis of pre-synaptic markers during development (Weinhard et al., 2018; Mordelt and de Witte, 2023). We chose to examine synapse phagocytosis at P30 because synaptic pruning has been reported to still be actively occurring in somatosensory cortex of mice at this timepoint (Cong et al., 2020). We chose the somatosensory cortex because we have previously found $P2Y_6R$ affects synaptic density in this area during aging (Dundee et al., 2023) and the somatosensory cortex affects working memory (Long and Zhang, 2021).

There was a small but significant increase in microglial Iba1 volume in the $P2Y_6R$ knockout mice compared to the wild-type mice (Fig. 1d, n=7-8, unpaired t-test, WT: 282, KO: 332, p=0.024, η^2=0.269), however there were no other observable effects on morphology (York et al., 2018), such as the number of branches (n=8, unpaired t-test, WT: 63, KO: 60, p=0.376, η^2=0.007), the number of branch points (n=8, unpaired t-test, WT: 52, KO: 50, p=0.391, η^2=0.006), the average branch length (n=8, unpaired t-test, WT: 32, KO: 33 p=0.327, η^2=0.015), or the maximum (n=8, unpaired t-test, WT: 70, KO: 71, p=0.393, η^2=0.005) and minimum (n=8, unpaired t-test, WT: 4.1, KO: 4.4, p=0.178, η^2=0.061) branch length (Fig. 2). Microglial density was subtly but significantly reduced in $P2Y_6R$ knockout mice suggesting a small effect on microglial proliferation at a young age (Fig. 3, n=8, unpaired t-test, WT: 54, KO: 49, p=0.007, η^2=0.357). There were no significant differences in microglial CD68 volume between wild-type and knockout mice (Fig. 1e, n=7-8, unpaired t-test, WT: 4.2, KO: 3.4, p=0.210, η^2=0.051), indicating no difference in microglial lysosomal volume. Note that virtually all of the CD68 staining was within Iba1-stained microglia (Extended Fig. 1-1), indicating that this marker of phagocytic lysosomes was relatively specific to microglia. Importantly, the volume of Vglut1 internalized within microglial CD68 was strongly and significantly lower in the knockout mice, indicating that the microglial phagocytosis of synapses is strongly reduced in knockout mice (Fig. 1f, n=7-8, unpaired t-test, WT: 0.028, KO: 0.007, p=0.001, η^2=0.506). This suggests that $P2Y_6R$ mediates the phagocytosis of synapses during development.

$P2Y_6R$ knockout results in increased synaptic density during development

In order to investigate whether this decrease in microglial phagocytosis of synapses had an effect on synapse density during development, we examined the synaptic density of wild-type and $P2Y_6R$ knockout mice at P30. Synaptic density was analyzed in the somatosensory cortex, the hippocampal CA1 and CA3 stratum radiatum, and the dentate gyrus molecular layer of P30 $P2Y_6R$ wild-type and knockout mice using confocal microscopy (Fig. 4a, 5a, 6a, and 7a). Coronal brain slices were immunostained using antibodies to Vglut1 (pre-synaptic marker) and Homer1 (post-synaptic marker), and synaptic density was measured as colocalized (<200 nm) puncta of both synaptic markers in an entire Z-stack.

In the somatosensory cortex, the density of Vglut1 puncta (n=8, unpaired t-test, WT: 100, KO: 105, p=0.030, η^2=0.229) and the colocalization of Vglut1 and Homer1 puncta (n=8, unpaired t-test, WT: 100, KO: 109, p=0.039, η^2=0.206) was significantly increased in knockout mice compared to wild-type mice, with no difference in Homer1 puncta density (Fig. 4b-d, n=8, unpaired t-test, WT: 100, KO: 101, p=0.418, η^2=0.003). No difference in density was observed in the hippocampal CA1 stratum radiatum for Vglut1 puncta (n=8, unpaired t-test, WT: 100, KO: 98, p=0.335,

η^2=0.013), Homer1 puncta (n=8, unpaired t-test, WT: 100, KO: 102, p=0.215, η^2=0.045), or the colocalization of Vglut1 and Homer1 puncta (Fig. 5b-d, n=8, unpaired t-test, WT: 100, KO: 101, p=0.394, η^2=0.005). In the hippocampal CA3 stratum radiatum, the density of Vglut1 puncta (n=8, unpaired t-test, WT: 100, KO: 108, p=0.038, η^2=0.208) and the colocalization of Vglut1 and Homer1 puncta (n=8, unpaired t-test, WT: 100, KO: 115, p=0.048, η^2=0.184) was significantly increased in knockout mice compared to wild-type mice, with no difference in Homer1 puncta (Fig. 6b-d, n=8, unpaired t-test, WT: 100, KO: 108, p=0.092, η^2=0.123). In the molecular layer of the dentate gyrus, the density of Homer1 puncta (n=8, unpaired t-test, WT: 100, KO: 114, p=0.005, η^2=0.388) and the colocalization of Vglut1 and Homer1 puncta (n=8, unpaired t-test, WT: 100, KO: 113, p=0.027, η^2=0.241) was significantly increased in knockout mice compared to wild-type mice, with no difference in Vglut1 puncta (Fig. 7b-d, n=8, unpaired t-test, WT: 100, KO: 100, p=0.485, η^2=0.0001). We did not examine synapse density in any other areas of the brain. Raw values for the Vglut1 puncta density, Homer1 puncta density, and the colocalization density are visible in Extended Figure 4-1. Furthermore, the Pearson correlation coefficient was calculated comparing the internalization of synaptic material per mouse in the somatosensory cortex to their corresponding synaptic density. We found a significant, negative correlation between the volume of internalized synaptic material by microglia and the synaptic density in the somatosensory cortex (Extended Fig. 4-2, n=15, Pearson correlation coefficient, r=-0.532, p=0.021). Altogether, these data indicate that $P2Y_6R$ knockout increases synapse density and decreases microglial phagocytosis of synapses during development, and the data are consistent with $P2Y_6R$-mediated microglial phagocytosis of synapses causing synaptic pruning during development.

$P2Y_6R$ knockout results in reduced memory

In the previous section, we found that $P2Y_6R$ knockout increased synapse density in the somatosensory cortex and hippocampus, regions that are associated with various forms memory (Rebola, Carta and Mulle, 2017; Hainmueller and Bartos, 2020; Long and Zhang, 2021). Dysregulated synaptic pruning during development has been associated with memory deficits (Wang et al., 2022). And we have previously observed a role for $P2Y_6R$-dependent memory loss in aging, and both an acute amyloid model and chronic tau model of neurodegeneration (Puigdellívol et al., 2021; Dundee et al., 2023).

To investigate whether the reduced synaptic pruning in $P2Y_6R$ knockout mice had a long-term effect on memory, we tested the memory of adult wild-type and $P2Y_6R$ knockout mice using the object location recognition test (OLRT), the novel object recognition test (NORT), and the Y-maze. The NORT tests object recognition memory (Ennaceur and Delacour, 1988) whilst the OLRT and Y-maze test spatial memory (Vogel-Ciernia and Wood, 2014; Kraeuter, Guest and Sarnyai, 2019). We first tested long-term spatial memory using the OLRT. 4-month-old mice were habituated in an open field for two consecutive days, and on the third day, mice were allowed to explore two identical objects for 10 min in the presence of visual clues on the walls of the open field. 24 h after this training, one of the objects remained in the same location (familiar) whilst the other was moved (novel), and the relative time spent with novel and familiar objects was quantified (Fig. 8a). During the training session, wild-type mice had no overall preference for the objects at either location (n=11, one-sample t-test to 50%, WT: 52, p=0.356, η^2=0.086) whilst $P2Y_6R$ knockout mice had a slight object preference (Fig. 8b, n=11, one-sample t-test to 50%, KO: 54, p=0.015, η^2=0.459). 24 h after training, wild-type mice spent more time with the object at the novel location, meaning they had long-term memory of the object locations (Fig. 8c, n=11, one-sample t-test to 50%, WT: 72, p=0.005, η^2=0.556). However, $P2Y_6R$ knockout mice did not show a preference for either object location (n=11, one-sample t-test to 50%, KO: 55, p=0.305, η^2=0.105) and showed reduced preference compared to wild-type mice (n=11, unpaired t-test, WT: 72, KO: 55, p=0.023, η^2=0.186), indicating that knockout mice have impaired long-term spatial memory.

Using the same animals, we then tested long-term recognition memory using the Novel Object Recognition Test (NORT). The animals had previously been habituauted in the open field (day 1 and 2) followed by the OLT (day 3 and 4). Visual clues were removed from the walls of the open field and on the fifth day mice were allowed to explore two new identical objects for 10 min. 24 h after training, one of the objects (familiar) was replaced by a new object (novel), and the relative time spent with novel and familiar objects was quantified (Fig. 8d). During the training session, both wild-type (n=11, one-sample t-test to 50%, WT: 56, p=0.033, η^2=0.379) and $P2Y_6R$ knockout (n=11, one-sample t-test to 50%, KO: 55, p=0.049, η^2=0.335) mice had a slight preference for one object (Fig. 8e). During the test, both wild-type (n=11, one-sample t-test to 50%, WT: 74, p=0.0002, η^2=0.770) and $P2Y_6R$ knockout (n=11, one-sample t-test to 50%, KO: 64, p=0.005, η^2=0.564) mice spent noticeably more time with the novel object, meaning they had long-term memory of the familiar object. However, $P2Y_6R$ knockout mice showed a significantly reduced preference for the novel object compared to wild-type mice (Fig. 8f, n=11, unpaired t-test, WT: 74, KO: 64, p=0.042, η^2=0.142), indicating that knockout mice have impaired long-term recognition memory. These data suggest that long-term memory is impaired in $P2Y_6R$ knockout mice.

We tested short-term spatial memory of 9-12-month old mice using the Y-maze, where mice were placed in the center of the symmetrical Y-maze and were allowed to explore freely for 8 min (Fig. 9a). The sequence, total number of arms entered, and distance traveled was recorded to determine the spontaneous alterations, which is a measure of short-term spatial memory. There was a non-significant increase in the number of total arm entries (Fig. 9b, n=7-9, unpaired t-test, WT: 34, KO: 46, p=0.064, η^2=0.157), and a significant increase in total distance travelled for $P2Y_6R$ knockout mice compared to wild-type mice (Fig. 9c, n=7-9, unpaired t-test, WT: 675, KO: 901, p=0.027, η^2=0.239), suggesting mildly increased motility of $P2Y_6R$ knockout mice. Both wild-type (n=9, one-sample t-test to 50%, WT: 72, p=0.0003, η^2=0.819) and $P2Y_6R$ knockout (n=7, one-sample t-test to 50%, KO: 60, p=0.010, η^2=0.691) mice carried out spontaneous alterations in the Y-maze, meaning both groups of mice had short-term spatial memory. However, there was a significant decrease in spontaneous alterations for $P2Y_6R$ knockout mice compared to wild-type mice, reduced from 72% in wild-type mice to 60% in $P2Y_6R$ knockout mice, where 50% indicates random arm entry and zero memory (Fig. 9d, n=7-9, unpaired t-test, WT: 72, KO: 60, p=0.013, η^2=0.304). This data indicates that $P2Y_6R$ knockout mice have impaired short-term spatial memory.

Finally, we tested short-term recognition memory of 9-12-month-old mice using the NORT. Mice were habituated in an open field for two consecutive days, and on the third day, mice were allowed to explore two identical objects for 10 min. 5 min after training, one of the objects (familiar) was replaced by a new object (novel), and the relative time spent with the novel and familiar objects was quantified (Fig. 9e). During the training session, both wild-type (n=7, one-sample t-test to 50%, WT: 50, p=0.919, η^2=0.002) and $P2Y_6R$ knockout (n=7, one-sample t-test to 50%, KO: 52, p=0.638, η^2=0.039) mice had no overall preference for either object (Fig. 9f). By contrast, during the test, both wild-type (n=7, one-sample t-test to 50%, WT: 72, p=0.001, η^2=0.860) and $P2Y_6R$ knockout (n=7, one-sample t-test to 50%, KO: 62, p=0.112, η^2=0.685) mice spent more time with the novel object, meaning they had short-term memory of the familiar object. However, $P2Y_6R$ knockout mice showed a significantly reduced preference for the novel object compared to wild-type mice (Fig. 9g, n=7, unpaired t-test, WT: 72, KO: 63, p=0.044, η^2=0.222), indicating that knockout mice have impaired short-term recognition memory. Overall, our data indicates that adult $P2Y_6R$ knockout mice have reduced memory, consistent with the reduced synaptic pruning during development resulting in long-term deficits in brain function.

Discussion

We had previously found that the $P2Y_6$ receptor ($P2Y_6R$) regulates microglial phagocytosis of synapses during aging in mice, by measuring microglial phagocytosis of isolated synapses, synaptic loss in culture, and synaptic internalization and loss *in vivo* (Dundee et al., 2023). We were therefore interested here in whether $P2Y_6R$ regulates microglial phagocytosis of synapses during development in mice, and if so, whether this affects adult brain function. We found here that $P2Y_6R$ knockout mice had greatly reduced synaptic material within microglial lysosomes, and increased synaptic density at postnatal day 30 (P30), consistent with $P2Y_6R$ regulating synaptic pruning. We found that adult $P2Y_6R$ knockout mice had impaired long- and short-term memory, consistent with reduced synaptic pruning causing memory dysfunction. Thus, it appears that $P2Y_6R$ mediates synaptic pruning via regulating microglial phagocytosis of synapses during development, and if this does not occur, adult brain dysfunction results. However, there are a number of uncertainties and limitations of our study that are outlined below.

We measured microglial phagocytosis of synapses as the internalization of the pre-synaptic marker Vglut1 into the CD68-stained lysosomes of Iba1-stained microglia in fixed sections of the somatosensory cortex of wild-type and $P2Y_6R$ knockout mice at P30. We found a large reduction in Vglut1 within microglial lysosomes in the knockout mice, consistent with reduced phagocytosis. This is consistent with previous research identifying a role for microglial phagocytosis in developmental synaptic pruning (Tremblay, Lowery, and Majewska, 2010; Paolicelli et al., 2011). However, we did not visualize/image phagocytosis over time, and it is conceivable that the reduced Vglut1 within microglial lysosomes in the knockout mice was due to increased digestion of the synaptic material within the knockout lysosomes. To directly test this possibility, in our previous publication, we fed isolated synapses (synaptosomes) to immortalized microglia and measured the rate of Vglut1 degradation with and without the $P2Y_6R$ inhibitor MRS2578 and found no difference in Vglut1 degradation rate (Dundee et al., 2023). Moreover, we showed that microglia isolated from $P2Y_6R$ knockout mice had a reduced rate of microglial phagocytosis of the isolated synapses (Dundee et al., 2023). Thus, the reduced Vglut1 within microglial lysosomes in the knockout mice found here is most likely due to reduced microglial phagocytosis of synapses. However, further experiments should be carried out on $P2Y_6R$ knockout microglial lysosomes to test for possible functional deficits, such as lysosomal acidity and enzyme composition.

We chose a pre-synaptic marker (Vglut1), rather than a post-synaptic marker, as there is clearer evidence for microglial phagocytosis of pre-synaptic markers during development (Weinhard et al., 2018; Mordelt and de Witte, 2023). However, it would be interesting to know whether $P2Y_6R$ also affects microglial phagocytosis of post-synaptic elements, such as dendritic spines, or the microglial phagocytosis of inhibitory synapses. We chose to examine synapse phagocytosis and density at P30 because synaptic pruning has been reported to still be actively occurring in somatosensory cortex of mice at this timepoint (Cong et al., 2020). However, it would be useful to know whether $P2Y_6R$ affects microglial phagocytosis at other developmental timepoints, including adults. We chose somatosensory cortex because there is evidence for a role in working memory and we have previously identified $P2Y_6R$-dependent phagocytosis occurring in this region (Long and Zhang, 2021; Dundee et al., 2023), but it would be informative to look at other areas of the brain.

We measured synapse density as the density of Vglut1-staining puncta, Homer1-staining puncta, and their co-localization (<200 nm) within the Z-stack of 25 μm thick brain sections using confocal microscopy. Thick sections have limitations with confocal microscopy, especially in relation to the z-plane (Avila and Henstridge, 2022), so ideally our data should be verified using array tomography of ultrathin sections. Vglut1 and Homer1 puncta density is high in the hippocampal stratum radiatum and molecular layer, as well as the somatosensory cortex, due to the high density of glutamatergic synapses. However, in the hippocampal stratum lacunosum-moleculare, Vglut1 puncta density is substantially lower compared to Vglut2 puncta density as Vglut2 is found primarily on output neurons in the hippocampus (Wozny et al., 2018). It may be beneficial to utilize excitatory synaptic markers that are less region specific for future studies, such as synaptophysin and PSD-95, as well as investigate inhibitory synapses. Note that we analyzed synapses at a single time point (P30) in mouse development, and it would be useful to analyze other time points in order to understand how $P2Y_6R$ affects changes in synapses during development.

We found a subtle increase in synaptic density in $P2Y_6R$ knockout mice, consistent with reduced microglial phagocytosis of synapses. However, this finding is also consistent with increased synaptogenesis or reduced retraction of synapses in the knockout mice. On the other hand, as there is clear evidence from us and others that $P2Y_6R$ mediates microglial phagocytosis (Koizumi et al., 2007; Puigdellívol et al., 2021; Dundee et al., 2023), but there is no evidence that $P2Y_6R$ affects synaptogenesis or synapse retraction. The most parsimonious explanation of our finding of increased synaptic density in the $P2Y_6R$ knockouts is reduced microglial phagocytosis of synapses, for which we have independent evidence. However, it would be useful to test the effect of $P2Y_6R$ knockout on other potential regulators of synaptic density. It would also be interesting to look at the effect of $P2Y_6R$ knockout on the density of particular synaptic types, such as inhibitory synapses.

We found that adult $P2Y_6R$ knockout mice had reduced short- and long-term memory, consistent with reduced synaptic pruning during development causing memory dysfunction. However, the memory defects of adult mice could result from reduced microglial phagocytosis of synapses in the adult mice, because such phagocytosis has been found to contribute to learning and memory in the adult brain (Miyanishi et al., 2021). This might be clarified by testing memory at earlier ages, or using conditional knockout of $P2Y_6R$. However, if learning and memory is regulated by $P2Y_6R$-dependent microglial phagocytosis of synapses, it may be difficult to disentangle a developmental effect from an adult effect. We have attributed the reduced memory of $P2Y_6R$ knockout mice to reduced synaptic pruning during development, however, it cannot be ruled out that the memory deficits result from other effects of $P2Y_6R$ yet to be discovered. We have previously reported that $P2Y_6R$ knockout mice have improved memory when 17 months old relative to wild-type mice, which have strongly degraded memory at this age (Dundee et al., 2023). We attributed this protection to $P2Y_6R$ mediating the excessive microglial phagocytosis of synapses occurring at this age (Dundee et al., 2023). Thus, $P2Y_6R$ regulated phagocytosis of synapses may potentially protect memory in the young and degrade memory in the old.

Disruption of synaptic pruning can lead to behavioral deficits in mice, reminiscent of neurodevelopmental disorders, such as autism and schizophrenia, suggesting that these disorders result from disrupted microglial phagocytosis of synapses (Faust, Gunner and Schafer, 2021; Mordelt and de Witte, 2023). It would therefore be interesting to test young $P2Y_6R$ knockout mice for behaviors, such as socialization, related to neurodevelopmental disorders. However, socialization deficits have been linked to specific neuronal-microglial signaling, such as via fractalkine (Corona et al., 2010), rather than microglia per se (Mordelt and de Witte, 2023). It is unclear what behavioral effects may result from loss of UDP-$P2Y_6R$ signaling but it would be interesting to investigate further.

$P2Y_6R$ is a receptor on microglia for extracellular UDP, and extracellular UDP acutely induces microglial phagocytosis (Koizumi et al., 2007). Kainate-stressed neurons have been shown to release UTP that is converted to UDP in the mouse brain (Koizumi et al., 2007), and amyloid beta-stressed neurons have also been shown to release UDP that activates $P2Y_6R$ (Puigdellívol et al., 2021). UTP is known to be released from stressed or apoptotic cells via pannexin or connexin channels (Elliott et al., 2009; Lazarowski, 2012). UDP activation of $P2Y_6R$ induces formation of the phagocytic cup in microglia, which is a late stage in the engulfment process, normally preceded by recognition of other phagocytic signals on the target. Thus, UDP-$P2Y_6R$ signaling may potentially combine with other signals to recognize synapses that should be engulfed (Cockram et al., 2021). It would be useful to test whether and in what conditions synapses release UDP (although this is currently difficult to do), and how UDP might combine with other signals on the synapse to regulate microglial phagocytosis of synapses.

Author contributions

JMD and MP managed the animal colonies. JMD analyzed the brain sections. RB wrote the puncta distribution analysis script. MP performed the 4-month-old behavioral studies. GCB conceived and managed the research. JMD and GCB wrote the manuscript. All authors reviewed and approved the manuscript.

Data availability statement

All code used to analyze synaptic puncta can be found at https://github.com/gurdon-institute/Synaptic-Density-Analysis. Experimental data reported in this paper will be shared by the corresponding authors upon request.

References

Avila, A.S. and Henstridge, C.M., 2022. Array tomography: 15 years of synaptic analysis. *Neuronal Signaling* [Online], 6(3), pp.2–11. Available from: https://doi.org/10.1042/ns20220013.

Cockram, T.O.J., Dundee, J.M., Popescu, A.S. and Brown, G.C., 2021. The Phagocytic Code Regulating Phagocytosis of Mammalian Cells. *Frontiers in Immunology* [Online], 12(June), pp.1–33. Available from: https://doi.org/10.3389/fimmu.2021.629979.

Cong, Q., Soteros, B.M., Wollet, M., Kim, J.H. and Sia, G.M., 2020. The endogenous neuronal complement inhibitor SRPX2 protects against complement-mediated synapse elimination during development. *Nature Neuroscience* [Online], 23(9), pp.1067–1078. Available from: https://doi.org/10.1038/s41593-020-0672-0.

Corona, A.W., Huang, Y., O'Connor, J.C., Dantzer, R., Kelley, K.W., Popovich, P.G. and Godbout, J.P., 2010. Fractalkine receptor (CX3CR1) deficiency sensitizes mice to the behavioral changes induced by lipopolysaccharide. *Journal of Neuroinflammation* [Online], 7. Available from: https://doi.org/10.1186/1742-2094-7-93.

Davis, R.A., Lii, K.-S. and Politis, D.N., 1956. Remarks on Some Nonparametric Estimates of a Density Function. *Selected Works of Murray Rosenblatt* [Online], pp.832–837. Available from: https://doi.org/10.1007/978-1-4419-8339-8_13.

Dundee, J.M., Puigdellívol, M., Butler, R., Cockram, T.O.J. and Brown, G.C., 2023. P2Y6 receptor-dependent microglial phagocytosis of synapses mediates synaptic and memory loss in aging. *Aging Cell* [Online], 22(2), pp.1–14. Available from: https://doi.org/10.1111/acel.13761.

Elliott, M.R., Chekeni, F.B., Trampont, P.C., Lazarowski, E.R., Kadl, A., Walk, S.F., Park, D., Woodson, R.I., Ostankovich, M., Sharma, P., Lysiak, J.J., Harden, T.K., Leitinger, N. and Ravichandran, K.S., 2009. Nucleotides released by apoptotic cells act as a find-me signal to promote phagocytic clearance. *Nature* [Online], 461(7261), pp.282–6. Available from: https://doi.org/10.1038/nature08296.

Ennaceur, A. and Delacour, J., 1988. A new one-trial test for neurobiological studies of memory in rats. 1: Behavioral data. *Behavioural Brain Research* [Online], 31(1), pp.47–59. Available from: https://doi.org/10.1016/0166-4328(88)90157-X.

Faust, T.E., Gunner, G. and Schafer, D.P., 2021. Mechanisms governing activity-dependent synaptic pruning in the developing mammalian CNS. *Nature Reviews Neuroscience* [Online], 22(11), pp.657–673. Available from: https://doi.org/10.1038/s41583-021-00507-y.

Gabandé-Rodríguez, E., Keane, L. and Capasso, M., 2020. Microglial phagocytosis in aging and Alzheimer's disease. *Journal of Neuroscience Research* [Online], 98(2), pp.284–298. Available from: https://doi.org/10.1002/jnr.24419.

Hainmueller, T. and Bartos, M., 2020. Dentate gyrus circuits for encoding, retrieval and discrimination of episodic memories. *Nature Reviews Neuroscience* [Online], 21(3), pp.153–168. Available from: https://doi.org/10.1038/s41583-019-0260-z.

Hong, S., Beja-Glasser, V.F., Nfonoyim, B.M., Frouin, A., Li, S., Ramakrishnan, S., Merry, K.M., Shi, Q., Rosenthal, A., Barres, B.A., Lemere, C.A., Selkoe, D.J. and Stevens, B., 2016. Complement and microglia mediate early synapse loss in Alzheimer mouse models. *Science* [Online], 352(6286), pp.712–716. Available from: https://doi.org/10.1126/science.aad8373.

Hong, S., Dissing-Olesen, L. and Stevens, B., 2016. New insights on the role of microglia in synaptic pruning in health and disease. *Current Opinion in Neurobiology* [Online], 36, pp.128–134. Available from: https://doi.org/10.1016/j.conb.2015.12.004.

Koizumi, S., Shigemoto-Mogami, Y., Nasu-Tada, K., Shinozaki, Y., Ohsawa, K., Tsuda, M., Joshi, B. V., Jacobson, K.A., Kohsaka, S. and Inoue, K., 2007. UDP acting at P2Y6 receptors is a mediator of microglial phagocytosis. *Nature* [Online], 446(7139), pp.1091–1095. Available from: https://doi.org/10.1038/nature05704.

Kraeuter, A.K., Guest, P.C. and Sarnyai, Z., 2019. The Y-Maze for Assessment of Spatial Working and Reference Memory in Mice. *Methods in Molecular Biology* [Online], 1916. Humana Press Inc., pp.105–111. Available from: https://doi.org/10.1007/978-1-4939-8994-2_10.

Lazarowski, E.R., 2012. Vesicular and conductive mechanisms of nucleotide release. *Purinergic Signalling* [Online], 8(3), pp.359–373. Available from: https://doi.org/10.1007/s11302-012-9304-9.

Long, X. and Zhang, S.J., 2021. A novel somatosensory spatial navigation system outside the hippocampal formation. *Cell Research* [Online], 31(6), pp.649–663. Available from: https://doi.org/10.1038/s41422-020-00448-8.

Milde, S., van Tartwijk, F.W., Vilalta, A., Hornik, T.C., Dundee, J.M., Puigdellívol, M. and Brown, G.C., 2021. Inflammatory neuronal loss in the substantia nigra induced by systemic lipopolysaccharide is prevented by knockout of the P2Y6 receptor in mice. *Journal of Neuroinflammation* [Online], 18(1), pp.1–9. Available from: https://doi.org/10.1186/s12974-021-02280-2.

Miyanishi, K., Sato, A., Kihara, N., Utsunomiya, R. and Tanaka, J., 2021. Synaptic elimination by microglia and disturbed higher brain functions. *Neurochemistry International* [Online], 142(October 2020), p.104901. Available from: https://doi.org/10.1016/j.neuint.2020.104901.

Mordelt, A. and de Witte, L.D., 2023. Microglia-mediated synaptic pruning as a key deficit in neurodevelopmental disorders: Hype or hope? *Current Opinion in Neurobiology* [Online], 79, p.102674. Available from: https://doi.org/10.1016/j.conb.2022.102674.

Moreno Manrique, J.F., Voit, P.R., Windsor, K.E., Karla, A.R., Rodriguez, S.R. and Beaudoin, G.M.J., 2021. SynapseJ: An Automated, Synapse Identification Macro for ImageJ. *Frontiers in Neural Circuits* [Online], 15(October), pp.1–17. Available from: https://doi.org/10.3389/fncir.2021.731333.

Murai, T., Okuda, S., Tanaka, T. and Ohta, H., 2007. Characteristics of object location memory in mice: Behavioral and pharmacological studies. *Physiology and Behavior* [Online], 90(1), pp.116–124. Available from: https://doi.org/10.1016/j.physbeh.2006.09.013.

Neher, J.J., Neniskyte, U., Hornik, T. and Brown, G.C., 2014. Inhibition of UDP/P2Y6 purinergic signaling prevents phagocytosis of viable neurons by activated microglia in vitro and in vivo. *Glia* [Online], 62(9), pp.1463–1475. Available from: https://doi.org/10.1002/glia.22693.

Otsu, N., Smith, P.L., Reid, D.B., Environment, C., Palo, L., Alto, P. and Smith, P.L., 1979. A Threshold Selection Method from Gray-Level Histograms. *IEEE Transactions on Systems, Man, and Cybernetics*, C(1), pp.62–66.

Prieur, E. and Jadavji, N., 2019. Assessing Spatial Working Memory Using the Spontaneous Alternation Y-maze Test in Aged Male Mice. *Bio-Protocol* [Online], 9(3), pp.1–10. Available from: https://doi.org/10.21769/bioprotoc.3162.

Puigdellívol, M., Milde, S., Vilalta, A., Cockram, T.O.J., Allendorf, D.H., Lee, J.Y., Dundee, J.M., Pampuščenko, K., Borutaite, V., Nuthall, H.N., Brelstaff, J.H., Spillantini, M.G. and Brown, G.C., 2021. The microglial P2Y6 receptor mediates neuronal loss and memory deficits in neurodegeneration. *Cell Reports* [Online], 37(13). Available from: https://doi.org/10.1016/j.celrep.2021.110148.

Paolicelli, R.C., Bolasco, G., Pagani, F., Maggi, L., Scianni, M., Panzanelli, P., Giustetto, M., Ferreira, T.A., Guiducci, E., Dumas, L., Ragozzino, D., Gross, C.T., 2010. Synaptic Pruning by Microglia is Necessary for Normal Brain Development. *Science*, 333, pp.1456-1459.

Rebola, N., Carta, M. and Mulle, C., 2017. Operation and plasticity of hippocampal CA3 circuits: Implications for memory encoding. *Nature Reviews Neuroscience* [Online], 18(4), pp.209–221. Available from: https://doi.org/10.1038/nrn.2017.10.

Schafer, D.P., Lehrman, E.K., Heller, C.T. and Stevens, B., 2014. An engulfment assay: A protocol to assess interactions between CNS phagocytes and neurons. *Journal of Visualized Experiments* [Online], (88), pp.1–12. Available from: https://doi.org/10.3791/51482.

Schafer, D.P., Lehrman, E.K., Kautzman, A.G., Koyama, R., Mardinly, A.R., Yamasaki, R., Ransohoff, R.M., Greenberg, M.E., Barres, B.A. and Stevens, B., 2012. Microglia Sculpt Postnatal Neural Circuits in an Activity and Complement-Dependent Manner. *Neuron* [Online], 74(4), pp.691–705. Available from: https://doi.org/10.1016/j.neuron.2012.03.026.

Schindelin, J., Arganda-Carreras, I., Frise, E., Kaynig, V., Longair, M., Pietzsch, T., Preibisch, S., Rueden, C., Saalfeld, S., Schmid, B., Tinevez, J.Y., White, D.J., Hartenstein, V., Eliceiri, K., Tomancak, P. and Cardona, A., 2012. Fiji: An open-source platform for biological-image analysis. *Nature Methods* [Online], 9(7), pp.676–682. Available from: https://doi.org/10.1038/nmeth.2019.

Sierra, A., Abiega, O., Shahraz, A. and Neumann, H., 2013. Janus-faced microglia: Beneficial and detrimental consequences of microglial phagocytosis. *Frontiers in Cellular Neuroscience* [Online], 7(JANUARY 2013), pp.1–22. Available from: https://doi.org/10.3389/fncel.2013.00006.

Stevens, B., Allen, N.J., Vazquez, L.E., Howell, G.R., Christopherson, K.S., Nouri, N., Micheva, K.D., Mehalow, A.K., Huberman, A.D., Stafford, B., Sher, A., Litke, A.M., Lambris, J.D., Smith, S.J., John, S.W.M., Barres, B.A., 2007. The classical complement cascade mediates CNS synapse elimination. *Cell*, 131(6), pp.1164-1178.

Tang, Y., Nyengaard, J.R., De Groot, D.M.G. and Gundersen, H.J.G., 2001. Total regional and global number of synapses in the human brain neocortex. *Synapse* [Online], 41(3), pp.258–273. Available from: https://doi.org/10.1002/syn.1083.

Tay, T.L., Béchade, C., D'Andrea, I., St-Pierre, M.K., Henry, M.S., Roumier, A. and Tremblay, M.E., 2018. Microglia gone rogue: Impacts on psychiatric disorders across the lifespan. *Frontiers in Molecular Neuroscience* [Online], 10(January), pp.1–26. Available from: https://doi.org/10.3389/fnmol.2017.00421.

Tremblay, M., Lowery, R.L., Majewska, A.K., 2010. Microglial Interactions with Synapses Are Modulated by Visual Experience. *PLoS Biology*, 8(11), pp.1-16.

Vogel-Ciernia, A. and Wood, M.A., 2014. Examining object location and object recognition memory in mice. *Current Protocols in Neuroscience* [Online], 2014, pp.8.31.1-8.31.17. Available from: https://doi.org/10.1002/0471142301.ns0831s69.

Wang, Y.Y., Deng, Y. Sen, Dai, S.K., Mi, T.W., Li, R.Y., Liu, P.P., Liu, C., He, B.D., He, X.C., Du, H.Z., Yang, H.C., Tang, Y., Liu, C.M. and Teng, Z.Q., 2022. Loss of microglial EED impairs synapse density, learning, and memory. *Molecular Psychiatry* [Online], 27(7), pp.2999–3009. Available from: https://doi.org/10.1038/s41380-022-01576-w.

Weinhard, L., Di Bartolomei, G., Bolasco, G., Machado, P., Schieber, N.L., Neniskyte, U., Exiga, M., Vadisiute, A., Raggioli, A., Schertel, A., Schwab, Y. and Gross, C.T., 2018. Microglia remodel synapses by presynaptic trogocytosis and spine head filopodia induction. *Nature Communications* [Online], 9(1). Available from: https://doi.org/10.1038/s41467-018-03566-5.

Wolf, S.A., Boddeke, H.W.G.M. and Kettenmann, H., 2017. Microglia in Physiology and Disease. *Annual Review of Physiology* [Online], 79, pp.619–643. Available from: https://doi.org/10.1146/annurev-physiol-022516-034406.

Wozny, C., Beed, P., Nitzan, N., Pössnecker, Y., Rost, B.R. and Schmitz, D., 2018. VGLUT2 functions as a differential marker for hippocampal output neurons. *Frontiers in Cellular Neuroscience* [Online], 12. Available from: https://doi.org/10.3389/fncel.2018.00337.

Xiao, X., Feng, Y.P., Du, B., Sun, H.R., Ding, Y.Q. and Qi, J.G., 2017. Antibody incubation at 37°c improves fluorescent immunolabeling in free-floating thick tissue sections. *BioTechniques* [Online], 62(3), pp.115–122. Available from: https://doi.org/10.2144/000114524.

York, E.M., Ledue, J.M., Bernier, L.P. and Macvicar, B.A., 2018. 3dmorph automatic analysis of microglial morphology in three dimensions from ex vivo and in vivo imaging. *eNeuro* [Online], 5(6). Available from: https://doi.org/10.1523/ENEURO.0266-18.2018.

Figure Legends

Figure 1: $P2Y_6R$ deficiency reduces synaptic pruning during development. (a) Representative confocal microscopy image of mice stained for Iba1 (green, microglial marker), CB68 (blue, lysosomal marker), and Vglut1 (red, synaptic marker) in the somatosensory cortex. Scale bar = 2 µm. Virtually all of the CD68 staining was within Iba1-stained microglia, as shown in Extended Figure 1-1. **(b)** Representative surface-rendered microglia (from a). Scale bar = 3 µm. **(c)** Enlarged inset of Vglut1 colocalization within CD68, denoted by the white dotted line (from b). Scale bar = 0.5 µm. Microglial volume **(d)**, CD68 volume within microglia **(e)**, and Vglut1 colocalization within CD68 **(f)** across P30 wild-type and $P2Y_6R$ knockout mice (n=7-8). Each point represents one animal comprised of 14–15 microglia analyzed across three equidistant sections. Statistical comparisons were made via unpaired t-tests. Error bars represent ±SEM, ns=p≥0.05, *p<0.05, **p<0.01.

Figure 2: $P2Y_6R$ deficiency does not affect microglial branching in the somatosensory cortex at P30. (a) Microglial branch end points identified by 3DMorph analysis (York et al., 2018). **(b)** Mean number of branch end points per microglia (n = 8). **(c)** Microglial branching points identified by 3DMorph analysis

(York et al., 2018). **(d)** Mean number of branching points per microglia (n = 8). **(e)** Mean branch length (µm) per microglia (n = 8). **(f)** Mean of the maximum branch length (µm) per microglia (n = 8). **(g)** Mean of the minimum branch length (µm) per microglia (n = 8). Each point represents one animal. Statistical comparisons were made via unpaired t-tests. Error bars represent ±SEM.

Figure 3: $P2Y_6R$ deficiency reduces microglial density in the somatosensory cortex at P30. (a) Representative fluorescent microscopy images of mice stained for Iba1 (green, microglial marker) and DAPI (blue, nuclei marker) in the somatosensory cortex. Scale bar = 50 µm. **(b)** Mean number of microglia per 20x field (n = 8). Each point represents one animal. Statistical comparison was made via an unpaired t-test. Error bars represent ±SEM, **p<0.01.

Figure 4: $P2Y_6R$ deficiency results in increased synaptic density in the somatosensory cortex. (a) Nissl stain from the Allen Mouse Brain Atlas and Allen Reference Atlas—Mouse Brain of a coronal section of the mouse brain, with the somatosensory cortex labeled. Available from: mouse.brain-map.org/static/atlas. **(b)** Colocalization of Vglut1 and Homer1 puncta. Scale bar = 0.5 µm. **(c)** Representative confocal microscopy images of P30 wild-type and $P2Y_6R$ knockout mice stained for Vglut1 (red, pre-synaptic marker), Homer1 (green, post-synaptic marker), and with DAPI (blue, nuclear stain) in the somatosensory cortex. Scale bar = 5 µm. **(d)** Vglut1 puncta density, Homer1 puncta density, and synaptic density of the somatosensory cortex (n = 8, 3 equidistant planes 300 µm apart per mouse). Synaptic density determined as colocalized Vglut1 and Homer1 puncta (<200 nm). Raw values for synaptic puncta density across brain regions are available in Extended Figure 4-1. Synaptic internalization by microglia negatively correlates with synaptic density in the somatosensory cortex, as shown in Extended Figure 4-2. Each point represents one animal. Statistical comparisons were made via unpaired t-tests. Error bars represent ±SEM, *p < 0.05.

Figure 5: $P2Y_6R$ deficiency does not affect synaptic density in the CA1 hippocampus. (a) Nissl stain from the Allen Mouse Brain Atlas and Allen Reference Atlas—Mouse Brain of a coronal section of the mouse brain, with the hippocampal CA1 stratum radiatum labeled. Available from: mouse.brain-map.org/static/atlas. **(b)** Colocalization of Vglut1 and Homer1 puncta. Scale bar = 0.5 µm. **(c)** Representative confocal microscopy images of P30 wild-type and $P2Y_6R$ knockout mice stained for Vglut1 (red, pre-synaptic marker), Homer1 (green, post-synaptic marker), and with

DAPI (blue, nuclear stain) in the hippocampal CA1 stratum radiatum. Scale bar = 5 µm. **(d)** Vglut1 puncta density, Homer1 puncta density, and synaptic density of the hippocampal CA1 stratum radiatum (n = 8, 3 equidistant planes 300 µm apart per mouse). Synaptic density determined as colocalized Vglut1 and Homer1 puncta (<200 nm). Each point represents one animal. Statistical comparisons were made via unpaired t-tests. Error bars represent ±SEM.

Figure 6: P2Y$_6$R deficiency results in increased synaptic density in the CA3 hippocampus. (a) Nissl stain from the Allen Mouse Brain Atlas and Allen Reference Atlas—Mouse Brain of a coronal section of the mouse brain, with the hippocampal CA3 stratum radiatum labeled. Available from: mouse.brain-map.org/static/atlas. **(b)** Colocalization of Vglut1 and Homer1 puncta. Scale bar = 0.5 µm. **(c)** Representative confocal microscopy images of P30 wild-type and P2Y$_6$R knockout mice stained for Vglut1 (red, pre-synaptic marker), Homer1 (green, post-synaptic marker), and with DAPI (blue, nuclear stain) in the hippocampal CA3 stratum radiatum. Scale bar = 5 µm. **(d)** Vglut1 puncta density, Homer1 puncta density, and synaptic density of the hippocampal CA3 stratum radiatum (n = 8, 3 equidistant planes 300 µm apart per mouse). Synaptic density determined as colocalized Vglut1 and Homer1 puncta (<200 nm). Each point represents one animal. Statistical comparisons were made via unpaired t-tests. Error bars represent ±SEM, *$p < 0.05$.

Figure 7: P2Y$_6$R deficiency results in increased synaptic density in the dentate gyrus. (a) Nissl stain from the Allen Mouse Brain Atlas and Allen Reference Atlas—Mouse Brain of a coronal section of the mouse brain, with the hippocampal dentate gyrus molecular layer labeled. Available from: mouse.brain-map.org/static/atlas. **(b)** Colocalization of Vglut1 and Homer1 puncta. Scale bar = 0.5 µm. **(c)** Representative confocal microscopy images of P30 wild-type and P2Y$_6$R knockout mice stained for Vglut1 (red, pre-synaptic marker), Homer1 (green, post-synaptic marker), and with DAPI (blue, nuclear stain) in the hippocampal dentate gyrus molecular layer. Scale bar = 5 µm. **(d)** Vglut1 puncta density, Homer1 puncta density, and synaptic density of the hippocampal dentate gyrus molecular layer (n = 8, 3 equidistant planes 300 µm apart per mouse). Synaptic density determined as colocalized Vglut1 and Homer1 puncta (<200 nm). Each point represents one animal. Statistical comparisons were made via unpaired t-tests. Error bars represent ±SEM, *$p < 0.05$.

Figure 8: P2Y$_6$R deficiency results in long-term memory loss. (a) Schematic representation of the training and testing sessions in the NORT. **(b)** Object

preference of each animal as percentage of time spent exploring two identical objects (n = 11). **(c)** Object preference of each animal as percentage of time spent exploring the novel object 24 h after training (n = 11). **(d)** Schematic representation of the training and testing sessions in the OLRT. **(e)** Object preference of each animal as percentage of time spent exploring two identical objects (n = 11). **(f)** Object preference of each animal as percentage of time spent exploring the novel object 24 h after training (n = 11). Data from (b) and (c) was reanalyzed from Dundee et al. (2023). Each point represents one animal. Dashed lines indicate a 50% chance level. Statistical comparisons were made via unpaired t-tests. Error bars represent ±SEM, $^*p < 0.05$.

Figure 9: P2Y$_6$R deficiency results in short-term memory loss. (a) Schematic representation of spontaneous alterations in the Y-maze. **(b)** Total number of arm entries by each animal in the Y-maze (n = 7-9). **(c)** Distance travelled (inches) by each animal in the Y-maze (n = 7-9). **(d)** Spontaneous alterations by each animal in the Y-maze (n = 7-9). **(e)** Schematic representation of the training and testing sessions in the NORT. **(f)** Object preference of each animal as percentage of time spent exploring two identical objects (n = 7). **(g)** Object preference of each animal as percentage of time spent exploring the novel object 24 h after training (n = 7). Data from (f) and (g) was reanalyzed from Puigdellívol et al. (2021). Each point represents one animal. Dashed lines indicate a 50% chance level. Statistical comparisons were made via unpaired t-tests. Error bars represent ±SEM, $^*p < 0.05$.

Extended Figure 1-1: CD68 staining is predominantly found within Iba1-positive microglia in the somatosensory cortex at P30. (a) Representative confocal microscopy images of mice stained for Iba1 (green, microglial marker) and CD68 (blue, lysosomal marker) in the somatosensory cortex. Scale bar = 10 µm. **(b)** Enlarged inset of CD68 colocalization within Iba1, denoted by the white dotted line (from a). White arrows indicate CD68 colocalization. Scale bar = 5 µm.

Extended Figure 4-1: Raw values for synaptic densities of the somatosensory cortex, CA1 hippocampal, CA3 hippocampal, and dentate gyrus regions of P30 mice. Vglut1 **(a)**, Homer1 **(b)**, and colocalization of Vglut1 and Homer1 **(c)** puncta densities in the somatosensory cortex (From Figure 4, n = 8, 3 equidistant planes 300 µm apart per mouse). Vglut1 **(d)**, Homer1 **(e)**, and colocalization of Vglut1 and Homer1 **(f)** puncta densities in the hippocampal CA1 stratum radiatum (From Figure 5, n = 8, 3 equidistant planes 300 µm apart per mouse). Vglut1 **(g)**, Homer1 **(h)**, and colocalization of Vglut1 and Homer1 **(i)** puncta densities in the hippocampal CA3 stratum radiatum (From Figure 6, n = 8, 3 equidistant planes 300 µm apart per mouse). Vglut1 **(j)**, Homer1 **(k)**, and colocalization of Vglut1 and Homer1 **(l)** puncta densities in the hippocampal dentate gyrus molecular layer (From Figure 7, n = 8, 3 equidistant planes 300 µm apart per mouse). Synaptic density determined as colocalized Vglut1 and Homer1 puncta (<200 nm). Each point represents one animal. Statistical comparisons were made via unpaired t-tests. Error bars represent ±SEM, *$p < 0.05$, **$p<0.01$.

Extended Figure 4-2: Synaptic internalization by microglia negatively correlates with synaptic density in the somatosensory cortex. Synaptic density of the somatosensory cortex (normalized to *P2ry6*$^{+/+}$ mice) plotted against volume of internalized synaptic material within microglia in the somatosensory cortex (n=15, WT=7, KO=8). Each point represents one animal. Statistical correlation was made by calculating the Pearson correlation coefficient.

Figure 1

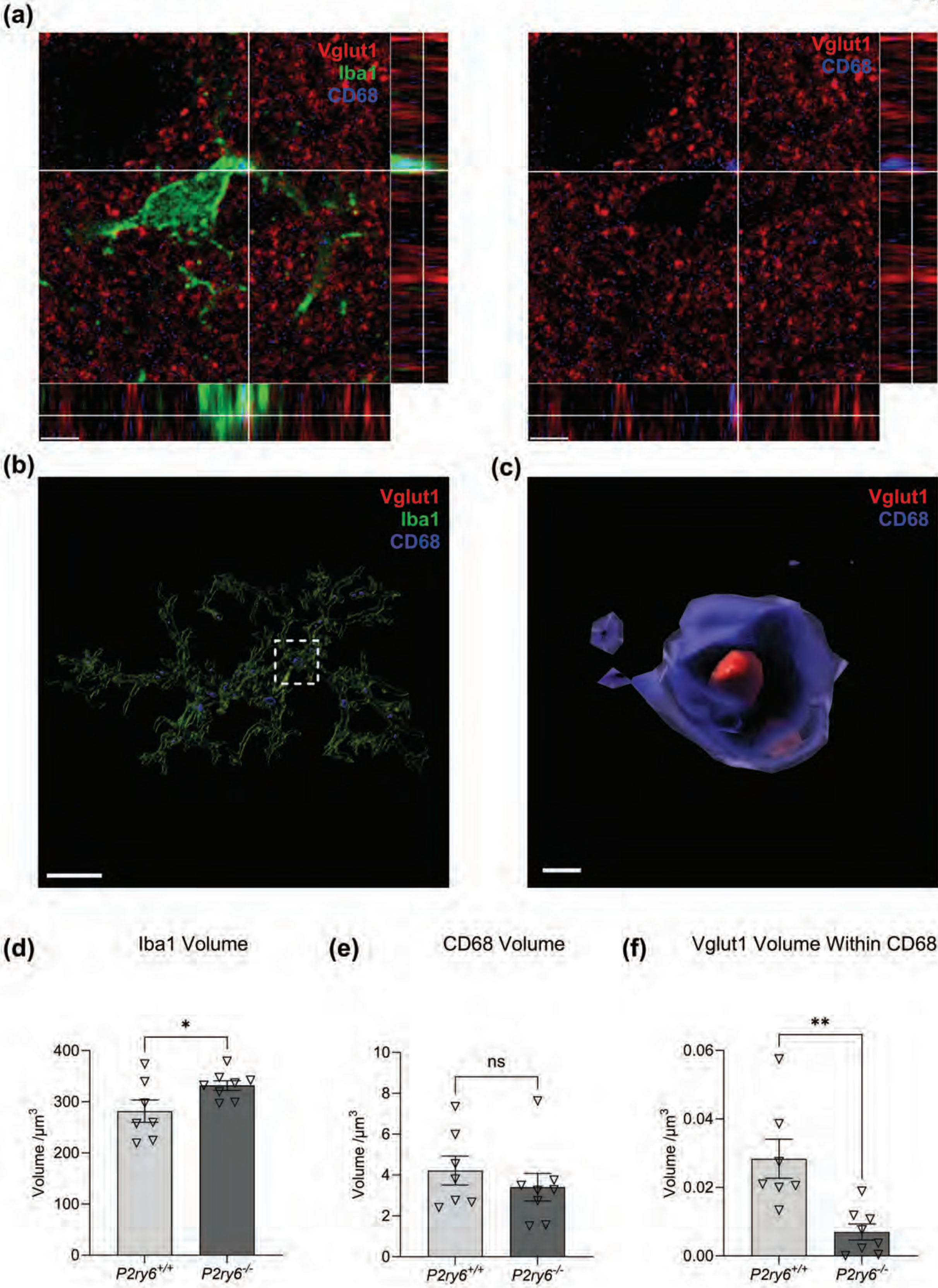
(a)
Vglut1
Iba1
CD68
Vglut1
CD68
(b)
Vglut1
Iba1
CD68
(c)
Vglut1
CD68
(d)
Iba1 Volume
*
400
300
200
100
0
Volume /μm3
P2ry6+/+
P2ry6-/-
(e)
CD68 Volume
ns
10
8
6
4
2
0
Volume /μm3
P2ry6+/+
P2ry6-/-
(f)
Vglut1 Volume Within CD68
**
0.06
0.04
0.02
0.00
Volume /μm3
P2ry6+/+
P2ry6-/-

Figure 2

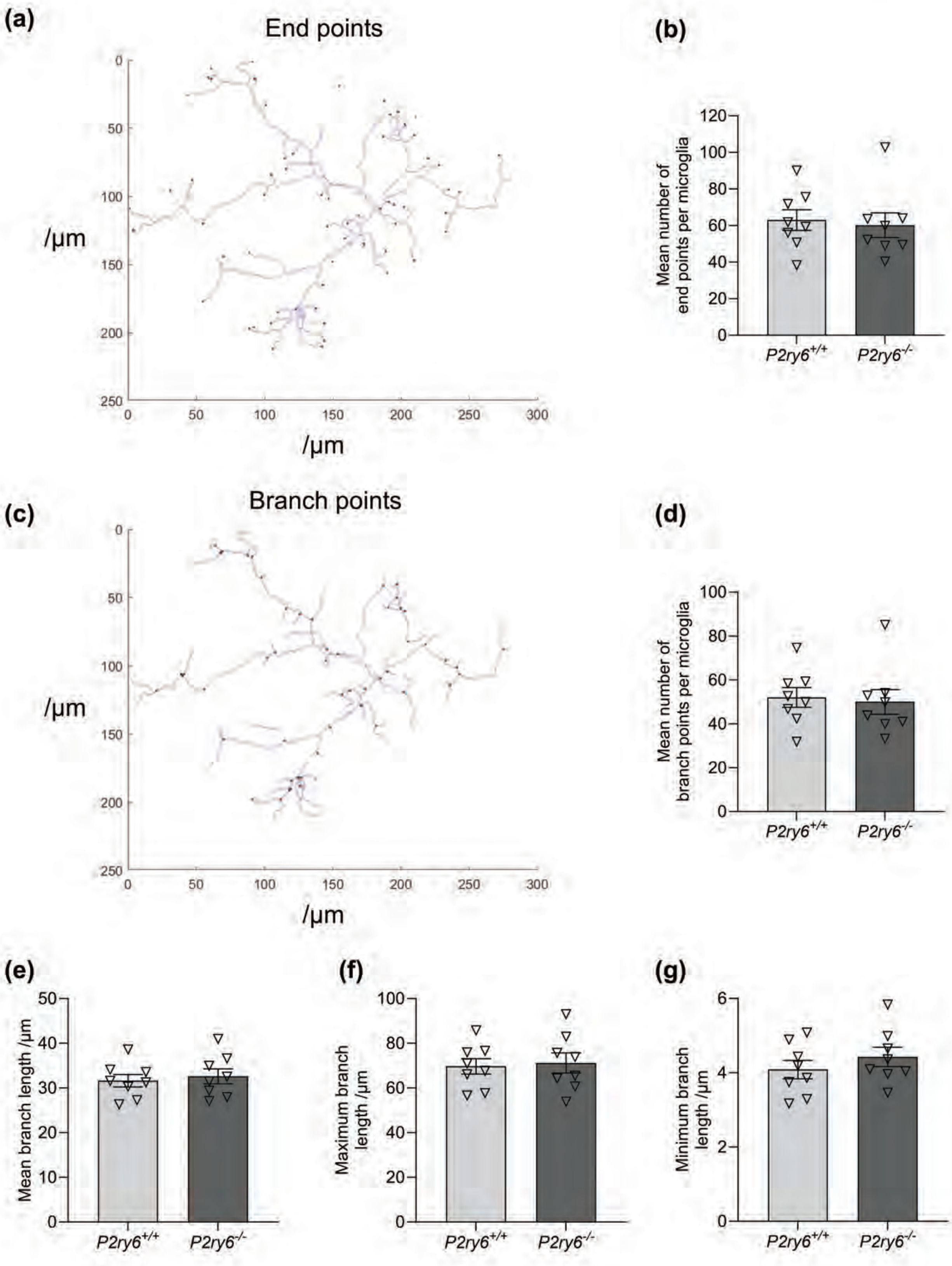
(a)
End points
/µm
/µm
(b)
Mean number of end points per microglia
P2ry6+/+
P2ry6-/-
(c)
Branch points
/µm
/µm
(d)
Mean number of branch points per microglia
P2ry6+/+
P2ry6-/-
(e)
Mean branch length /µm
P2ry6+/+
P2ry6-/-
(f)
Maximum branch length /µm
P2ry6+/+
P2ry6-/-
(g)
Minimum branch length /µm
P2ry6+/+
P2ry6-/-

Figure 3

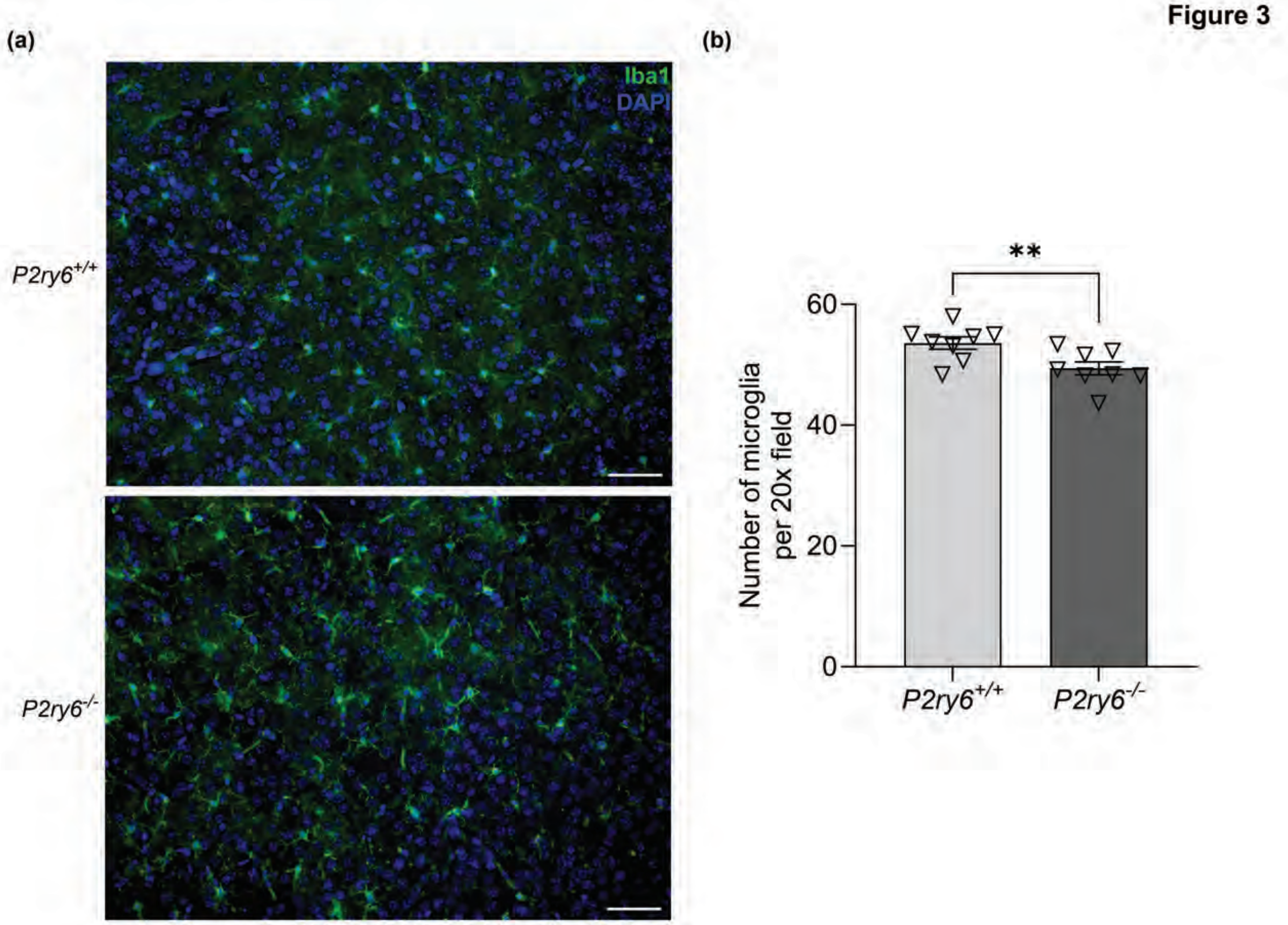
(a)
Iba1
DAPI
P2ry6+/+
P2ry6-/-
(b)
**
Number of microglia per 20x field
60
40
20
0
P2ry6+/+
P2ry6-/-

Figure 4

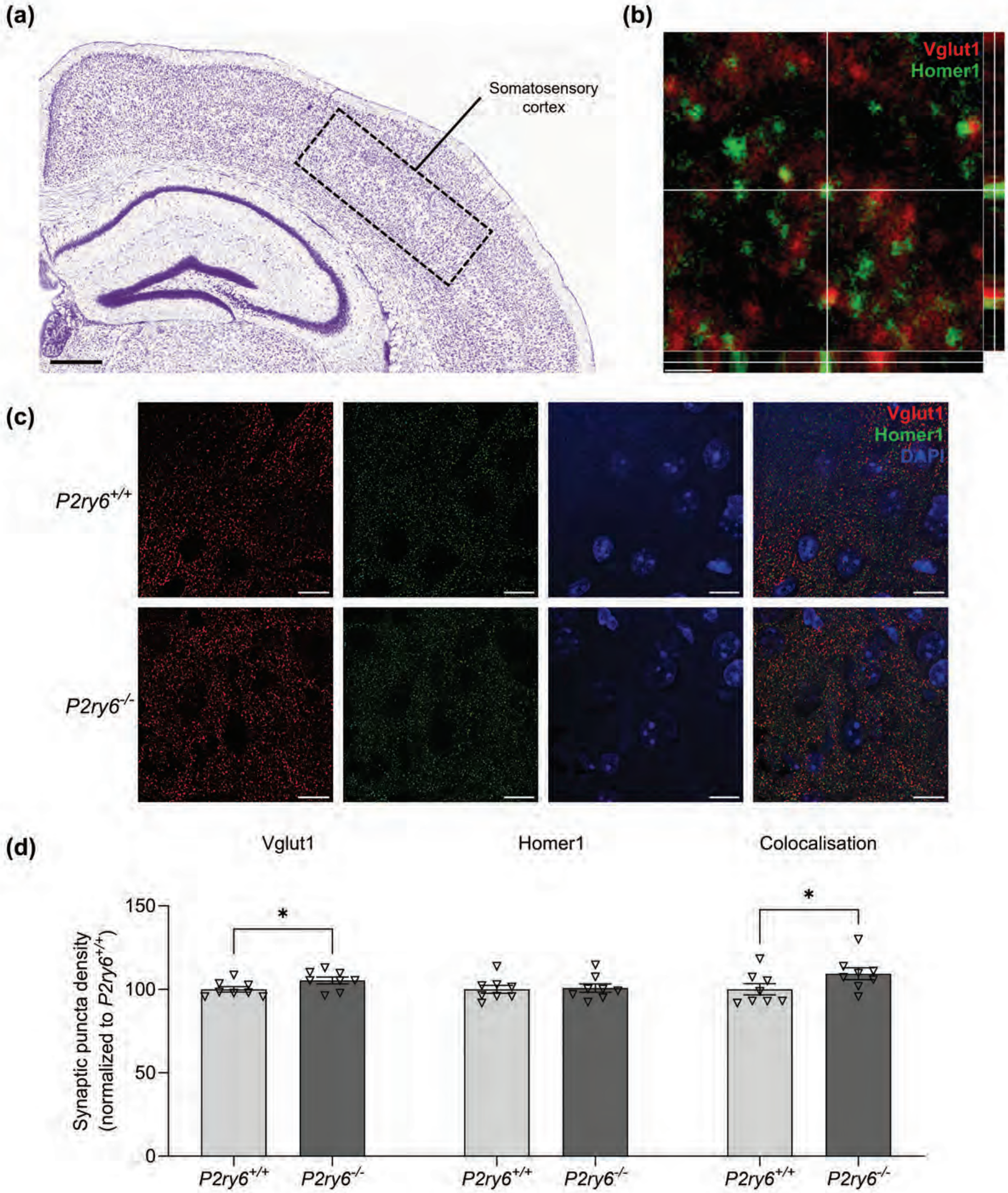

(a)
Somatosensory cortex
(b)
Vglut1
Homer1
(c)
Vglut1
Homer1
DAPI
P2ry6+/+
P2ry6-/-
(d)
Vglut1
Homer1
Colocalisation
Synaptic puncta density (normalized to P2ry6+/+)
150
100
50
0
*
*
P2ry6+/+
P2ry6-/-
P2ry6+/+
P2ry6-/-
P2ry6+/+
P2ry6-/-

Figure 5

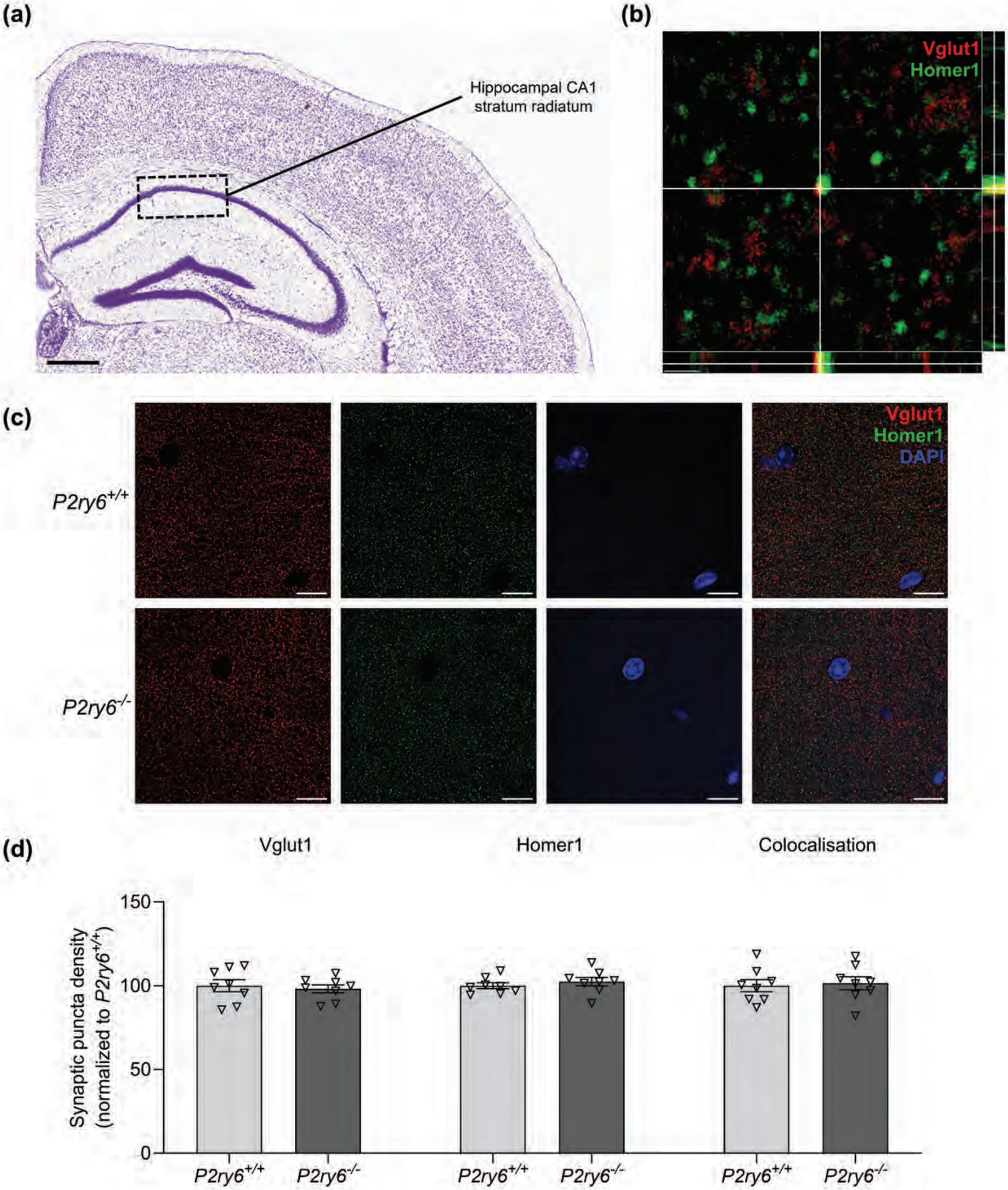
(a)
Hippocampal CA1
stratum radiatum
(b)
Vglut1
Homer1
(c)
Vglut1
Homer1
DAPI
P2ry6+/+
P2ry6-/-
(d)
Vglut1
Homer1
Colocalisation
Synaptic puncta density
(normalized to P2ry6+/+)
150
100
50
0
P2ry6+/+
P2ry6-/-
P2ry6+/+
P2ry6-/-
P2ry6+/+
P2ry6-/-

Figure 6

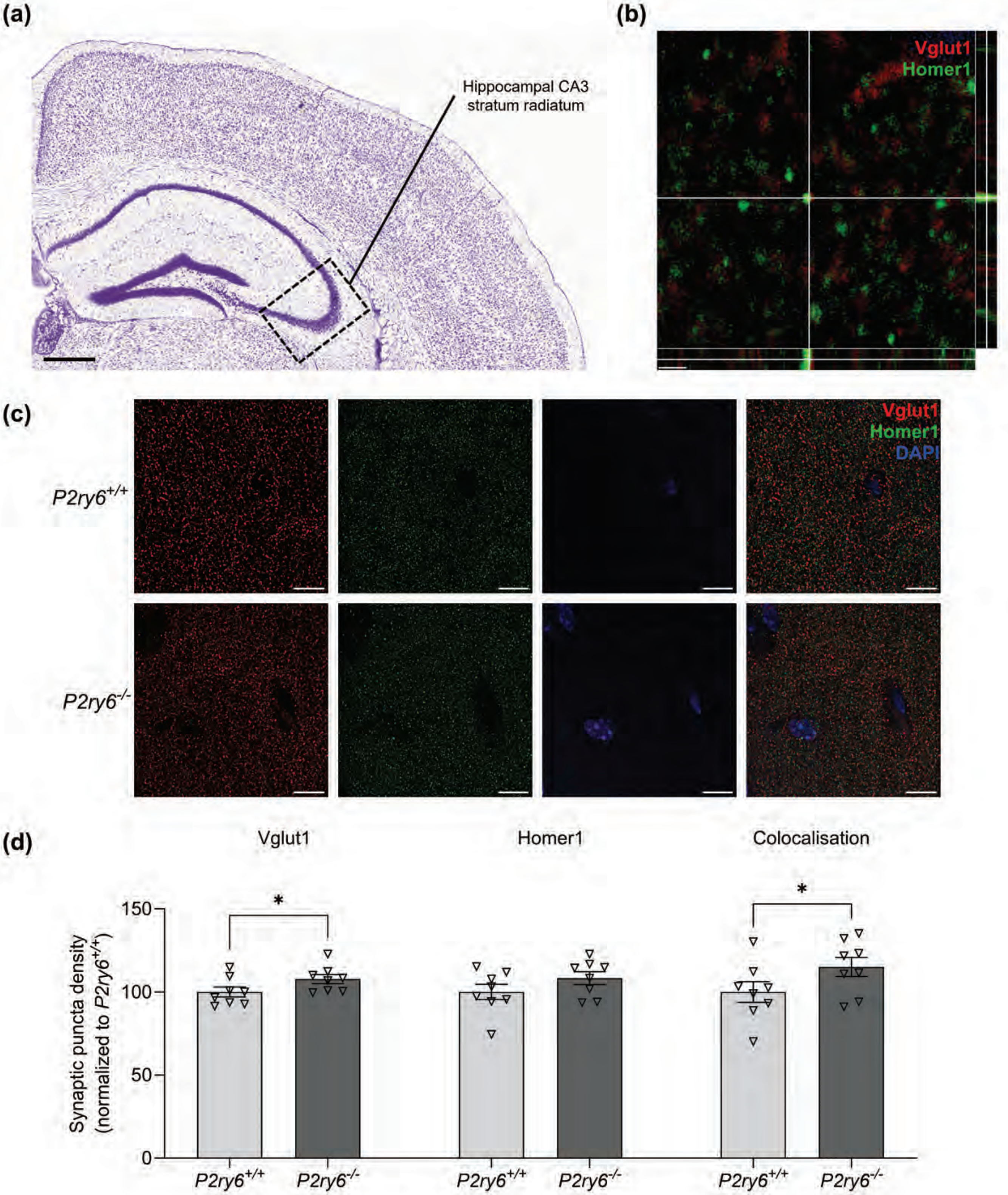
(a)
Hippocampal CA3
stratum radiatum
(b)
Vglut1
Homer1
(c)
Vglut1
Homer1
DAPI
P2ry6+/+
P2ry6-/-
(d)
Vglut1
Homer1
Colocalisation
Synaptic puncta density
(normalized to P2ry6+/+)
150
100
50
0
*
*
P2ry6+/+
P2ry6-/-
P2ry6+/+
P2ry6-/-
P2ry6+/+
P2ry6-/-

Figure 7

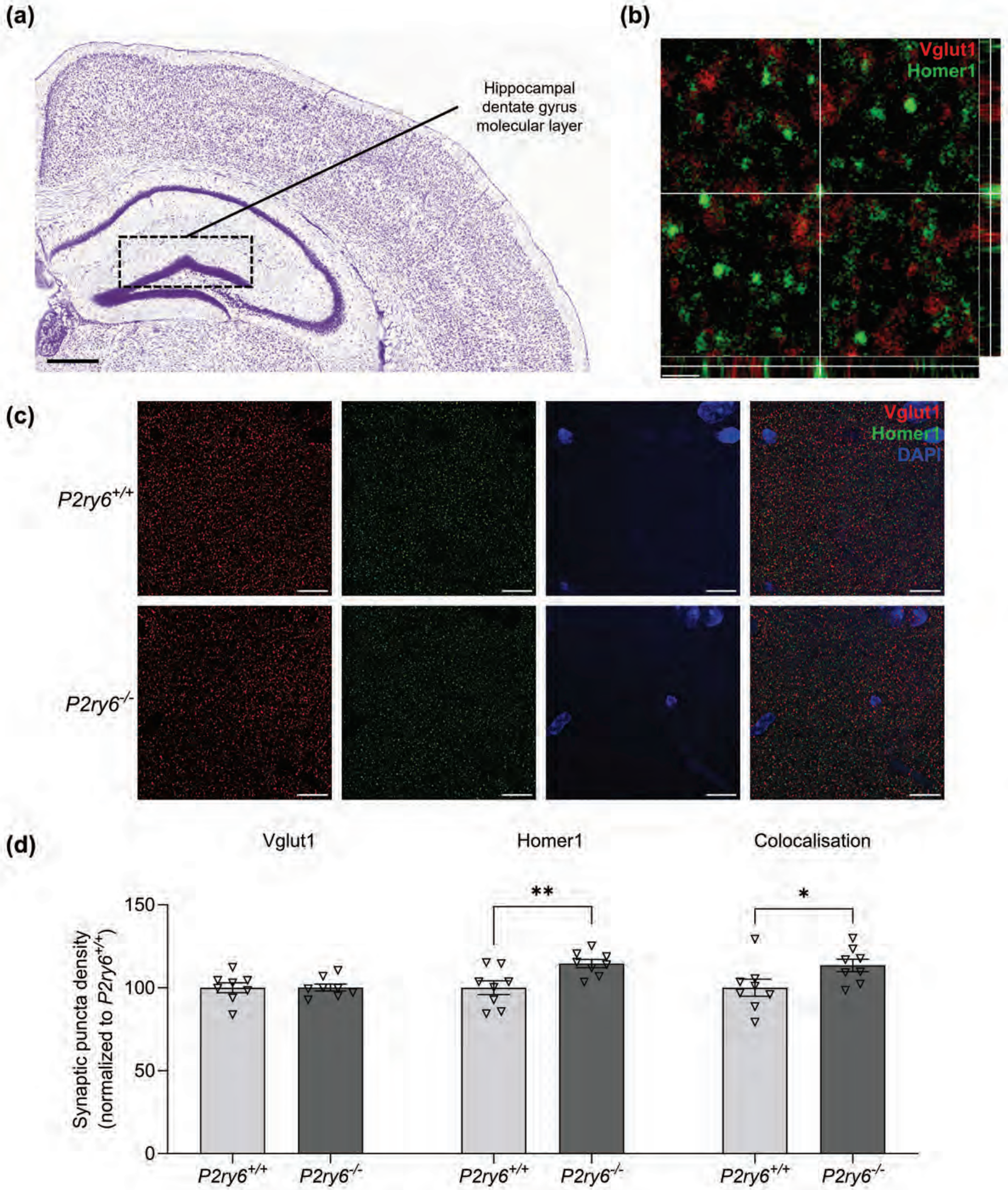
(a)
Hippocampal dentate gyrus molecular layer
(b)
Vglut1
Homer1
(c)
Vglut1
Homer1
DAPI
P2ry6+/+
P2ry6-/-
(d)
Vglut1
Homer1
Colocalisation
**
*
Synaptic puncta density (normalized to P2ry6+/+)
150
100
50
0
P2ry6+/+
P2ry6-/-
P2ry6+/+
P2ry6-/-
P2ry6+/+
P2ry6-/-

Figure 8

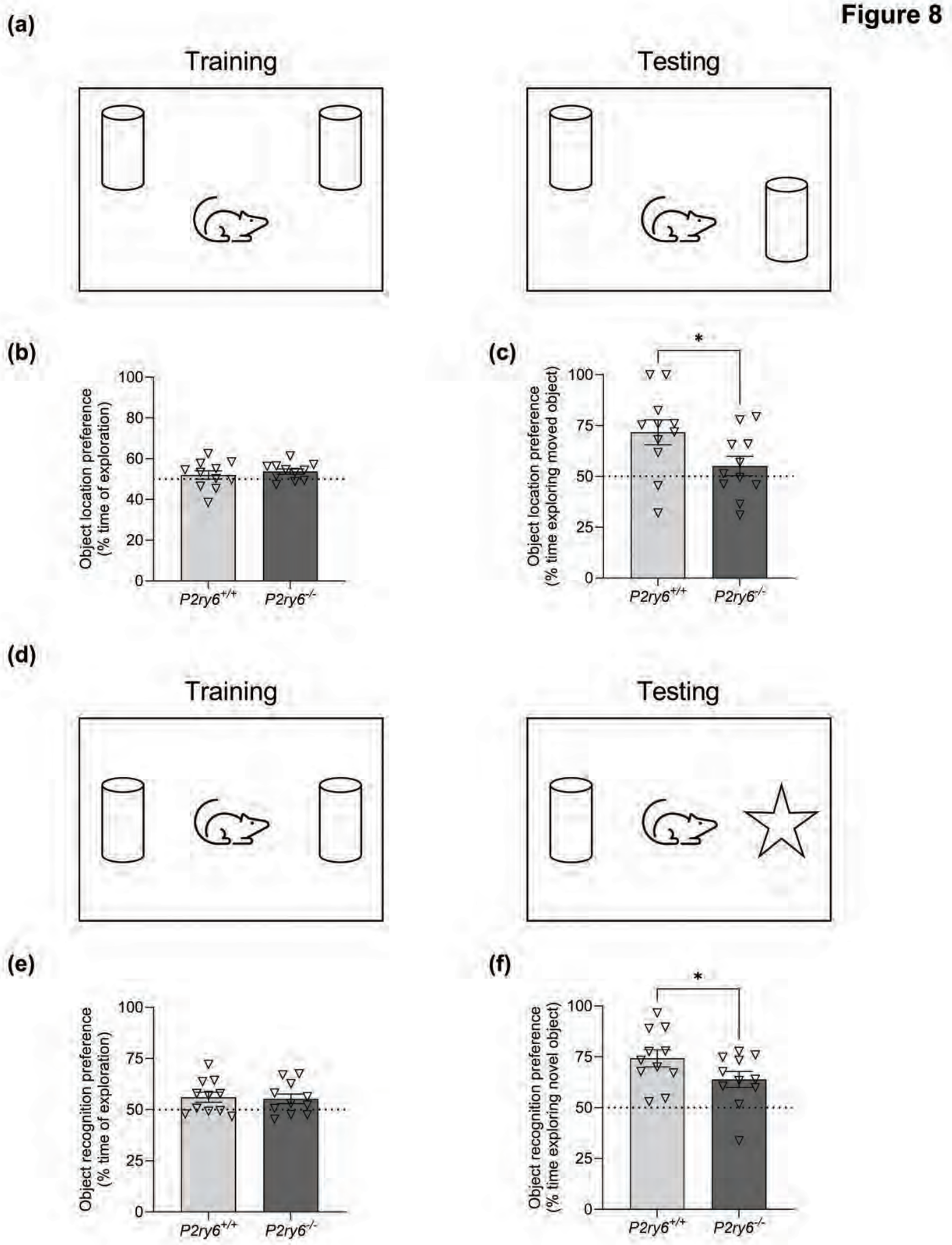
(a)
Training
Testing
(b)
Object location preference
(% time of exploration)
100
80
60
40
20
0
P2ry6+/+
P2ry6-/-
(c)
*
Object location preference
(% time exploring moved object)
100
75
50
25
0
P2ry6+/+
P2ry6-/-
(d)
Training
Testing
(e)
Object recognition preference
(% time of exploration)
100
75
50
25
0
P2ry6+/+
P2ry6-/-
(f)
*
Object recognition preference
(% time exploring novel object)
100
75
50
25
0
P2ry6+/+
P2ry6-/-

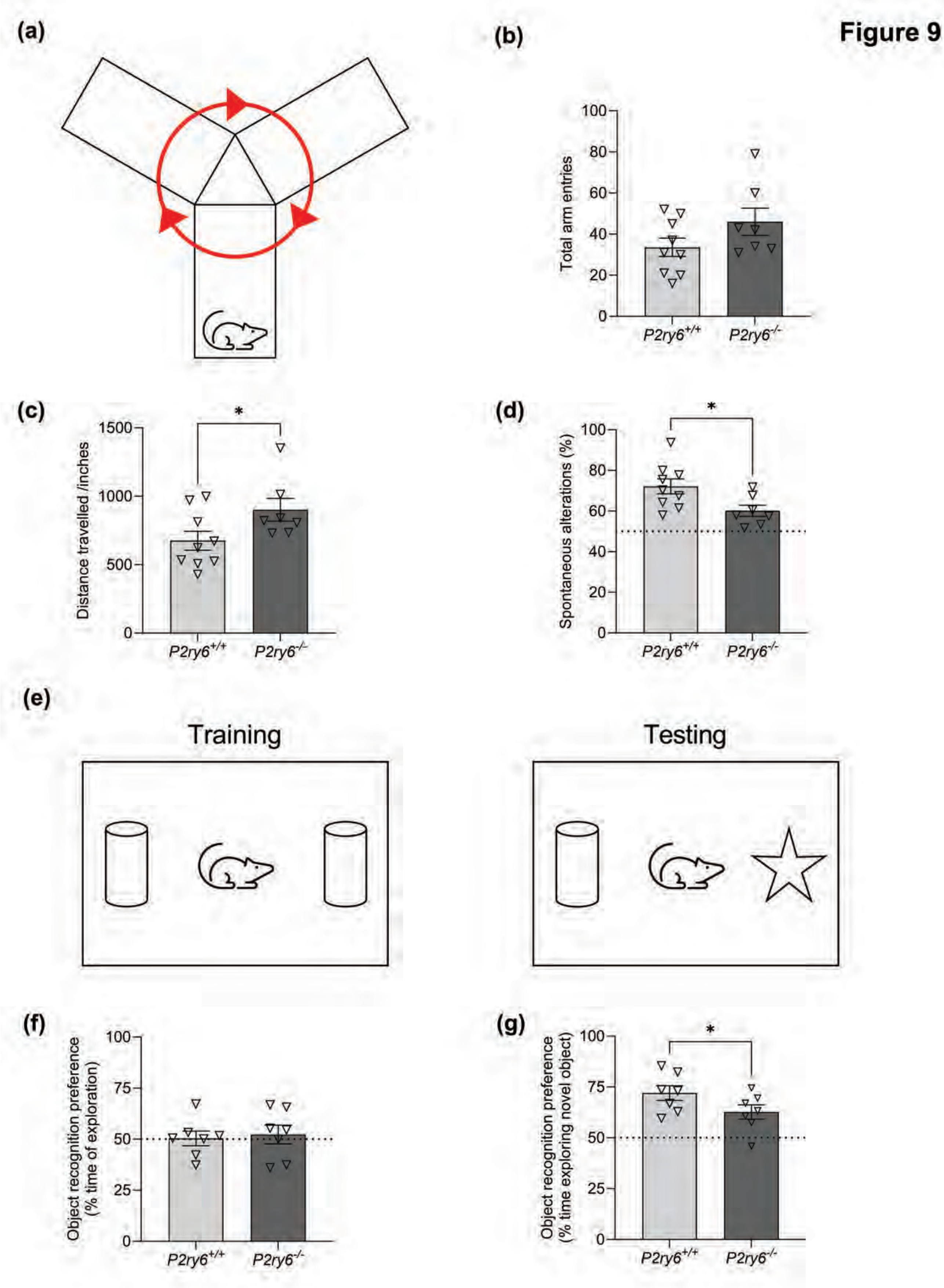
Figure 9
(a)
(b)
Total arm entries
100
80
60
40
20
0
P2ry6+/+
P2ry6-/-
(c)
Distance travelled /inches
1500
1000
500
0
*
P2ry6+/+
P2ry6-/-
(d)
Spontaneous alterations (%)
100
80
60
40
20
0
*
P2ry6+/+
P2ry6-/-
(e)
Training
Testing
(f)
Object recognition preference (% time of exploration)
100
75
50
25
0
P2ry6+/+
P2ry6-/-
(g)
Object recognition preference (% time exploring novel object)
100
75
50
25
0
*
P2ry6+/+
P2ry6-/-